Impact of optically induced carriers on the spin relaxation of localized electron spins in isotopically enriched silicon

M. Beck,[1] N. V. Abrosimov,[2] J. Hübner,[1] and M. Oestreich[1]
[1]*Institut für Festkörperphysik, Leibniz Universität Hannover, 30167 Hannover, Germany*
[2]*Leibniz-Institut für Kristallzüchtung, 12489 Berlin, Germany*

(Received 13 March 2019; published 3 June 2019)

We investigate the influence of Auger electrons on the efficiency of optical spin pumping of donor bound electrons in isotopically enriched silicon by means of time-resolved pump-probe absorption spectroscopy. The experimentally observed drastic shortening of the spin relaxation time with increasing optical excitation results from inelastic scattering between free and localized electrons and an interconnected Orbach-type spin relaxation process. The maximal steady-state degree of polarization of the localized electron spins and the probe-beam-induced depolarization dynamics reveal that the fast, nonthermal energy dissipation of the conduction band electron distribution is detrimental for efficient optical spin initialization. In fact, each absorbed photon creates an Auger electron with enough energy to depolarize the spin of ≈30 donor bound electrons but the fast, nonthermal energy dissipation by phonons reduces this spin relaxation efficiency to approximately unity.

DOI: 10.1103/PhysRevB.99.245201

Donor bound electrons in isotopically enriched ^{28}Si may be the key to a silicon-based quantum information technology [1]. The donor bound electron (D^0) and the donor nucleus have extraordinarily long spin coherence times in ^{28}Si [2,3] and can be efficiently initialized by optical pumping [4]. The spins can be manipulated individually by electrical means [5] but the ultranarrow line widths of the donor bound exciton transitions (D^0X) enable also the combination of conventional nuclear magnetic and electron spin resonance techniques with individual optical addressability [6,7]. Such optical means provide manifold opportunities in the context of silicon-based quantum information technology whereat one crucial key figure for prospective implementations is the intrinsic limit of the optical spin pumping efficiency.

The efficient optical pumping and manipulation of the electron spin system via the D^0X transition has been compellingly demonstrated in several experiments and relies upon the D^0X Auger recombination. The Auger recombination is the dominating D^0X recombination channel in silicon [8] and pumps the optically addressed bound electron after resonant optical D^0X excitation high into the conduction band. The spin information is lost during this process since the D^0X hole spin relaxation is much faster than the Auger recombination time, i.e., the two electrons of the D^0X trion have the same probability to recombine with the optically excited hole. Thereby, resonant optical pumping of a spin specific D^0 transition depopulates the respective D^0 spin population with 50% efficiency promising optical spin initialization with very high purity. However, the same Auger electrons responsible for spin pumping also scatter via Coulomb interaction with the D^0 ensemble reducing the D^0 ensemble spin lifetime by an Orbach-type process.

In the following, we study this intrinsic interplay of optical D^0 spin pumping and D^0 spin relaxation via Auger electrons by time-resolved pump-probe absorption spectroscopy. We quantitatively describe the complete low-temperature spin and charge dynamics of the optically pumped D^0X system by the rate-equation model depicted in Fig. 1, trace the undesirable, optically induced D^0 spin relaxation back to Auger excitation of the D^0 $1S$-A_1 to T_2 transition, and extract as key parameter the intrinsic efficiency of inelastic scattering of the Auger electrons with the D^0 [9].

The optical pumping experiments are carried out on a 4 mm long ^{28}Si sample, which is isotopically enriched to 99.994% and n doped with a nominal phosphorus doping concentration of $n_d = 1.2 \times 10^{15}$ cm^{-3}. The sample is placed strain free at 4.5 K in a specially designed helium gas reservoir coupled to the cold finger of a cryogen-free refrigerator [10]. Application of a transverse magnetic field of 50 mT leads to a splitting of the donor ground state into four levels according to the Breit-Rabi equation for the bound electron and the phosphorus nucleus as two spin-1/2 particles. The D^0X state is split into four levels by the Zeemann splitting of the trion's spin-3/2 hole. Figure 1(left) depicts schematically the resulting level diagram and the twelve dipole allowed optical transitions, i.e., six doublet transitions each split by half of the phosphorus donor hyperfine coupling constant $A = 117.53$ MHz [11]. The D^0 are polarized in the following experiment by pumping the energetically overlapping doublet 9/10 by a frequency stabilized external cavity diode laser [12] at a transition photon energy where experimentally the maximum degree of electron spin polarization is observed. We measure the resulting electron spin polarization by scanning the probe laser across the doublets 5/6 and 7/8, which have identical oscillator strengths but different donor electron spin orientation and are therefore ideally suited to monitor the degree of polarization. In contrast to previous studies of the D^0X, which employed photoluminescence excitation spectroscopy, we directly measure the absorption of the zero phonon D^0X transition, which quantitatively yields the optical excitation rate. In order to enhance the signal-to-noise ratio of the weak absorption signal, we phase modulate the probe

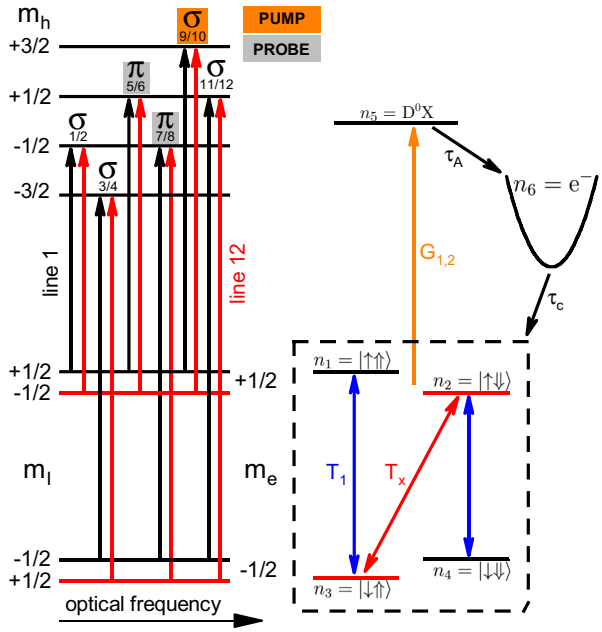

FIG. 1. (left) Level diagram of the dipole allowed D^0X transitions in an external magnetic field and the employed pump (orange) and probe (light gray) transitions. (right) Schematic diagram of the electron spin polarization process. Depicted are (the population of) the four possible donor spin states n_1 to n_4, the donor bound exciton states n_5, the conduction band n_6, as well as the relevant excitation and relaxation channels.

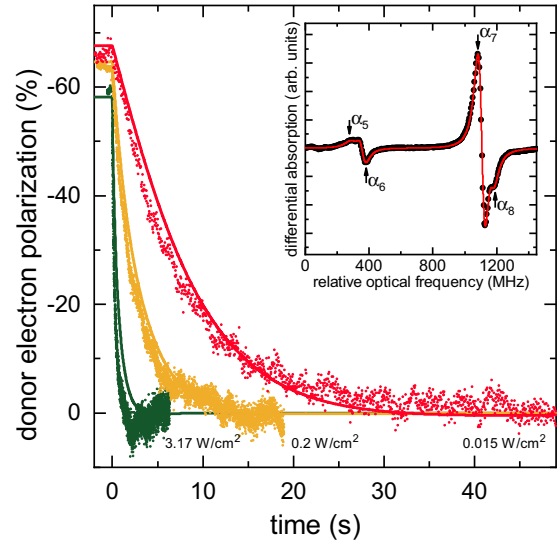

FIG. 2. Temporal change of the initial D^0 polarization after the pump laser is turned off at $t = 0$ s for different probe intensities (colored dots). The corresponding solid lines are the results of the numerical model including the dependence of T_1 on excitation density. (Inset) Typical differential probe absorption spectrum of the D^0X transitions 5–8 according to Fig. 1 for a pump intensity of 1.7 mW. The black dots are measured and the red line is the corresponding line shape fit with four differential Lorentzians. The absolute frequency corresponding to the origin of the frequency axis is 278.032 005(1) THz.

laser with a fiber-based, broadband electro-optic modulator at $\Omega = 3.2$ MHz and detect the differential absorption by a high-frequency lock-in amplifier. The radius of the probe laser is 86(3) μm $1/e^2$ and of the pump 224(5) μm for all experiments. The inset of Fig. 2 shows a typical steady-state differential absorption spectrum for a pump and probe intensity of 1700 μW and 5.7 μW, respectively. A cumulative line shape analysis consisting of the sum of the four differential Lorentzian contributions, which are fitted to the distinct spectra, yields a polarization of $P = -68(1)\%$ where the polarization P is defined in terms of the intensity I_i of the respective absorption line i as

$$P = \frac{(I_5 + I_6) - (I_7 + I_8)}{I_5 + I_6 + I_7 + I_8}. \quad (1)$$

The same degree of polarization is obtained if the polarization is just evaluated by the absolute value of the depicted differential absorption local extrema α_5 to α_8.

In the next step, we measure the temporal dynamics of these four local extrema of the differential absorption in dependence on probe power by a time-resolved pump-probe technique. First, we create the maximal steady-state polarization of the D^0 by optical pumping the doublet 9/10. Then, the pump beam is shut off by a fast mechanical shutter, which defines $t = 0$, and we measure with the continuously present probe beam the time-resolved transient of one of the α_i by the fast lock-in amplifier with a time resolution of ≈1.5 ms. This procedure is repeated many times for each α_i and each probe power in order to increase the signal-to-noise ratio. Figure 2 shows exemplary the resulting time traces of the extracted D^0 polarization for three different probe intensities. The measurements show clearly that the polarization decay becomes faster with increasing probe intensity. Figure 3 shows as black dots the extracted measured polarization decay times, which

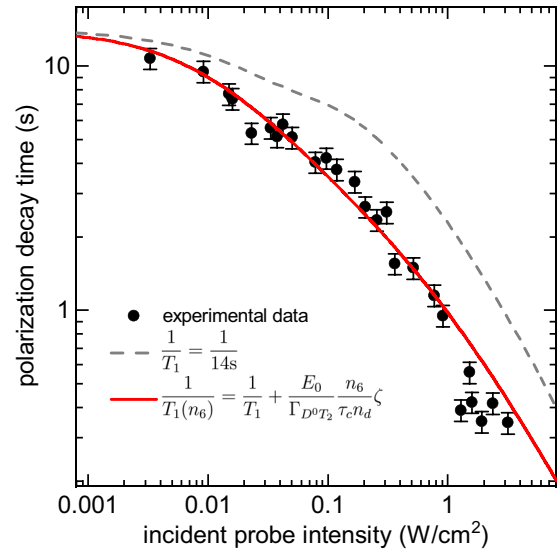

FIG. 3. Measured polarization decay time in dependence on optical probe intensity (black symbols). The dashed gray line is a simulation based on the numerical model with $T_1 = 14$ s. The solid red line is calculated including the Orbach-type process due to hot Auger electrons [see Eq. (5)].

have been extracted by a single exponential decay fit to the respective polarization time trace for probe intensities ranging over three orders of magnitude. The polarization decay time decreases from 10.2 s for the lowest probe intensity to 270 ms for the highest intensity.

The modeling of the spin and carrier dynamics with rate equations reveals in the following that this faster decay not only results from the faster depopulation of the pump-induced initial spin population but also from the interaction of the hot Auger electrons in the conduction band with the D^0. The basic mechanism of D^0 spin polarization by optical pumping is outlined in Ref. [4] and illustrated in Fig. 1 (right). Here, n_1 to n_4 denote the population of the D^0 ground-state levels with the four possible spin combinations of $\pm\frac{1}{2}$ electron spin and $\pm\frac{1}{2}$ nuclear spin of the phosphorus atom, n_5 is the population of the optically excited D^0X level, and n_6 of the unpolarized free conduction band electrons resulting from the Auger recombination of the D^0X. The difference in population of $n_{1,2,3,4}$ at thermal equilibrium can be neglected since the energy splitting of $n_{1,2,3,4}$ is much smaller than k_BT. Optical excitation by the pump and probe lasers transfers the occupancy of D^0 selectively from $n_{1,2,3,4}$ to n_5. The respective generation rates per donor $G_{1,2,3,4}$ of the pump and probe lasers are readily calculated from the measured absorption coefficients, which yields the overall rate of absorbed photons. The spot sizes of the focused laser beams are used to normalize the rates by the number of donors inside the volume spanned by the probe laser or pump laser, respectively. The D^0X recombines after excitation by Auger recombination with the Auger decay time $\tau_A = 272$ ns [8]. The resulting unpolarized conduction band Auger electron relaxes its energy before being captured by an ionized phosphorus impurity with the rate

$$\tau_c^{-1} = \sigma_c \cdot v \cdot (n_6 + n_{d,i}), \tag{2}$$

where $\sigma_c \cdot v$ is the effective electron capture volume per time of a single phosphorus donor and $n_6 + n_{d,i}$ is the total number of ionized donors. This total number consists of the number of ionized donors in our n-type sample at thermal equilibrium due to partial compensation by p-type background doping, $n_{d,i} \approx 10^{14}\,\mathrm{cm}^{-3}$, plus the number of donors ionized by optical excitation. The latter is equal to the number of Auger electrons in the conduction band, i.e., n_6. The rate $\tau_c^{-1} = 6$ GHz is in very good approximation constant since $n_6 \ll n_{d,i}$ for all applied pump and probe intensities. Finally, the resulting spin polarization of the D^0 decays either by the longitudinal spin relaxation time T_1 or by the cross relaxation time T_x. The longitudinal electron spin relaxation time of the undisturbed system is ≈14 s at a lattice temperature of 4.5 K [13]. The cross relaxation rate between the states n_2 and n_3 coupled by hyperfine interaction is calculated as

$$T_\mathrm{x}^{-1} = \sin(\theta/2)^2(G_2 + G_3), \tag{3}$$

where $\sin(\theta/2)^2$ is the probability of a spin flip for each ionization event of the neutral donor [14], $\theta = \arctan[A/(\gamma^+ B)]$, and $\gamma^+ \approx 28\,\mathrm{GHzT}^{-1}$ is the sum of the electron and the nuclear gyromagnetic ratios. The resulting coupled differential equations for the complete dynamics of the optically driven D^0 system read:

$$\frac{d}{dt}n_1(t) = -G_1 \cdot n_1(t) + \frac{n_6(t)}{4 \cdot \tau_c} - \frac{n_1(t) - n_3(t)}{2 \cdot T_1}, \quad \frac{d}{dt}n_4(t) = -G_4 \cdot n_4(t) + \frac{n_6(t)}{4 \cdot \tau_c} - \frac{n_4(t) - n_2(t)}{2 \cdot T_1}, \tag{4a}$$

$$\frac{d}{dt}n_2(t) = -G_2 \cdot n_2(t) + \frac{n_6(t)}{4 \cdot \tau_c} - \frac{n_2(t) - n_4(t)}{2 \cdot T_1} - \frac{n_2(t) - n_3(t)}{2 \cdot T_\mathrm{x}}, \tag{4b}$$

$$\frac{d}{dt}n_3(t) = -G_3 \cdot n_3(t) + \frac{n_6(t)}{4 \cdot \tau_c} - \frac{n_3(t) - n_1(t)}{2 \cdot T_1} - \frac{n_3(t) - n_2(t)}{2 \cdot T_\mathrm{x}}, \tag{4c}$$

$$\frac{d}{dt}n_5(t) = G_1 \cdot n_1(t) + G_2 \cdot n_2(t) + G_3 \cdot n_3(t) + G_4 \cdot n_4(t) - \frac{n_5(t)}{\tau_A}, \quad \frac{d}{dt}n_6(t) = \frac{n_5(t)}{\tau_A} - \frac{n_6(t)}{\tau_c}. \tag{4d}$$

We calculate the steady-state polarization and the polarization decays shown in Fig. 2 by solving the set of differential equations [(4a)–(4d)] taking into account the outlined experimental protocol [15]. The dashed gray line in Fig. 3 shows the calculated D^0 spin polarization decay time for a constant $T_1 = 14$ s, i.e., neglecting the influence of Auger electrons on T_1 [16]. Such a constant T_1 clearly underestimates the probe-beam-induced decay of D^0 spin polarization.

The Auger electron in the conduction band has an initial excess energy of about 1.1 eV while the D^0 $1S$-A_1 to T_2 interband transition relevant for the Orbach-type process has an energy of $\Delta = 11.6$ meV [17]. If all the Auger electron excess energy were transferred into heating of the D^0 ensemble, each excited Auger electron would lead to an Orbach-type spin relaxation of many D^0 making any efficient optical D^0 spin initialization impossible. Accordingly, the really important parameter for optically assisted spin quantum information processing in ^{28}Si is the number of D^0 $1S$-A_1 to T_2 interband transitions per Auger electron, ζ. This parameter can be readily extracted by a fit to the measured polarization decay time depicted in Fig. 3 by the rate equation model including optically induced Orbach-type spin relaxation by

$$\frac{1}{T_1(n_6)} = \frac{1}{T_1} + \frac{E_0}{\Gamma_{D^0T_2}} \frac{n_6}{\tau_c n_d} \zeta, \tag{5}$$

where $T_1 = 14$ s is the known phonon induced spin relaxation time at 4.5 K [13], $E_0 \approx 3 \times 10^8\ \mathrm{s}^{-1}$ is the Orbach constant [13], and $\Gamma_{D^0T_2} = 1.02$ GHz is the D^0 T_2 to $1S$-A_1 electron relaxation rate [18]. In Eq. (5) $E_0/\Gamma_{D^0T_2}$ denotes the probability that a D^0 $1S$-A_1 to T_2 interband transition leads to electron spin relaxation, and $n_6/(\tau_c n_d)$ is the number of excited Auger electrons per second normalized to the density of donors, which yields by multiplication with ζ the D^0 $1S$-A_1 to T_2

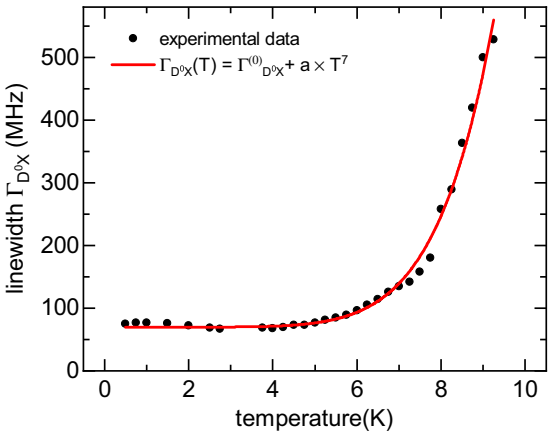

FIG. 4. Full width at half maximum of the measured linewidth Γ_{D^0X} of the D^0X transition versus lattice temperature. The solid line is a fit according to $\Gamma_{D^0X}(T) = \Gamma^{(0)}_{D^0X} + a \times T^7$ with $\Gamma^{(0)}_{D^0X} = 70(3)$ MHz.

excitation rate. Fitting the experimental decay times in Fig. 3 with ζ being the only fitting parameter yields $\zeta = 3.2$, which is in surprisingly good agreement with estimations from the carrier cooling dynamics presented in the Appendix. The same ζ also yields excellent agreement for the initial degree of spin polarization produced by pump and probe beam as evidenced in Fig. 2. Obviously, an increasing ζ would asymptotically lead to a vanishing steady-state polarization. However, the calculations of the carrier cooling dynamics in silicon suggests that ζ is in good approximation independent of the D^0 doping density for a wide range of doping concentrations.

Finally, we want to point out that the experiments presented in this paper consistently exhibit a homogeneous broadening of the D^0X transitions, which is *inter alia* a major requirement for corresponding prospective quantum information devices. We have therefore checked for all employed laser intensities between 0.003 and 3 W/cm^2 that the line shape of the D^0X transition is in very good approximation Lorentzian [19]. The rather large homogeneous broadening at 4.5 K exceeds any remaining inhomogeneous broadening effects in the current sample, e.g., due to residual ^{29}Si isotopes, and might result from a direct or cross interaction of neutral and ionized D^0. We can exclude heating of the lattice by Auger electrons or by residual laser absorption as possible cause since the measured D^0X absorption spectrum is an extremely accurate lattice thermometer [20]. Thermal excitation of the D^0 $1S$-A_1 to T_2 transition can also be ruled out since this process would show up in the D^0 spin relaxation time. We have additionally measured the broadening of the D^0X transitions at $B = 0\,T$ in dependence on temperature and find a T^7 increase with increasing temperature as shown in Fig. 4. Such a temperature dependence has been measured before, e.g., in rare-earth doped ceramics [21], and is characteristic for the homogeneous broadening by elastic Raman scattering with phonons.

In conclusion, we have studied the transient pumping dynamics of D^0 spins in isotopically pure ^{28}Si, which is a promising candidate for spin quantum information processing. The dynamics can be described by an amazingly unpretentious theoretical model and allows a quantitative understanding of the underlying optical pumping process. The study reveals that optical spin pumping inevitably leads to Orbach-type spin relaxation of the donor bound electrons reducing the spin initialization efficiency. The reduction of the longitudinal spin relaxation time in dependence on excitation density is universally valid for all optical pumping powers and D^0 densities relevant for this kind of silicon-based optical quantum information technology. Each excited Auger electron activates $\approx$3.2 D^0 $1S$-A_1 to T_2 interband transitions, which corresponds to the situation where the optically induced Orbach-type spin relaxation rate becomes comparable to the spin pumping rate. Only two deviations are expected. First, an increase of the p-type background doping close to the phosphorus doping density reduces the effective energy transfer to the D^0 ensemble and thereby reduces the Orbach process enabling in principle a more efficient spin initialization. Second, very high doping densities result in neutral impurity scattering times comparable to the cooling dynamics by optical phonons, increase the energy transfer to the D^0 ensemble, and thereby increase spin relaxation. Such high doping densities play a role for example in certain electrical spin injection measurements. The physical model is also applicable to prospective quantitative optical spin injection experiments [22] where the D^0 transition is used as sensitive optical spin detector.

ACKNOWLEDGMENTS

We gratefully acknowledge financial support from the NTH School for Contacts in Nanosystems and funding by the German Science Foundation (DFG) via cluster of excellence "QuantumFrontiers" (EXC 2123), research training group RTG 1991, and Project No. OE 177/10-1.

APPENDIX

Here, we present the relevant scattering rates and the energy loss dynamics of those D^0 electrons that are excited by Auger recombination from the D^0X trion state into the conduction band. The calculations show for our n-doped bulk ^{28}Si sample that the energy relaxation of these Auger electrons is dominated for the first 2 ps by phonon emission while subsequently inelastic D^0 impurity scattering takes over. The theoretically estimated number of D^0 $1S$-A_1 to T_2 interband transitions per Auger electron, ζ, corroborates the experimental result presented in the main text.

Energy relaxation dynamics

The electron density in the conduction band, n_6, resulting from the D^0X Auger recombination depends on the laser intensity and the capture time τ_c and ranges in our case between $n_6 \approx 3 \times 10^3\,\mathrm{cm}^{-3}$ and $n_6 \approx 10^5\,\mathrm{cm}^{-3}$. The corresponding electron-electron scattering rates can be roughly approximated by $10^{-5}\,\mathrm{cm}^{-3}\,\mathrm{s}^{-1} \cdot n_6$ [24] and are therefore negligible in comparison to all other relevant scattering rates, i.e., the conduction band electrons do not thermalize by electron-electron scattering, which simplifies the following calculations.

The Auger electrons from the D^0X recombination start with an initial excess energy of about 1.10(1) eV at $t = 0$ in the conduction band. The fastest energy relaxation processes

TABLE I. Parameters for the calculation of the Auger electron cooling dynamics.

$(D_tK)_{g,LO}$	11×10^8 eV cm^{-1}	[27]
ϵ_{LO}	62.0 meV	[27]
$(D_tK)_{g,LA}$	2×10^8 eV cm^{-1}	[27]
ϵ_{LA}	47.4 meV	[27]
$(D_tK)_{f,TO}$	2×10^8 eV cm^{-1}	[27]
ϵ_{TO}	59.0 meV	[27]
Ξ_0^2	9 eV	[27]
Ξ_1^2	5.6 eV	[25]
n_d	1.2×10^{15} cm^{-3}	
$n_{d,i}$	10^{14} cm^{-3}	

are in this case g and f scattering by TO, LO, and LA phonons, which can be calculated for low lattice temperatures by [24]

$$\left(\frac{dE}{dt}\right)_{\text{inter}} = \frac{Z_i (D_tK)_i^2 m_e^{3/2}}{\sqrt{2}\pi\hbar^2\rho}\tilde{N}_q\sqrt{E-\epsilon_i}, \tag{A1}$$

where $(D_tK)_i$ is the interband deformation potential for the phonon type i with energy ϵ_i, $\tilde{N}_q = N_q + 1$ is the phonon occupation number, and ρ is the density of the crystal. The factor Z_i is either 1 for g scattering or 4 for f scattering. The emission of optical phonons takes place on a sub 100 fs timescale and is completed after about 2 ps. We further include first-order scattering by so called 190 K acoustic phonons with $\epsilon_1 = k_B 190$ K [25] by the energy relaxation rate

$$\left(\frac{dE}{dt}\right)_{\text{inter},1} = \frac{\Xi_1^2 (2\cdot m_e)^{5/2}}{2\pi\hbar^4\rho}\tilde{N}_q\sqrt{E-\epsilon_1}\cdot\left(E-\frac{\epsilon_1}{2}\right). \tag{A2}$$

After about 2 ps the energy loss is governed by two concurring processes. The first one is intravalley scattering with acoustic phonons with the corresponding rate

$$\left(\frac{dE}{dt}\right)_{\text{intra}} = \frac{\Xi_0^2 (2\cdot m_e)^{5/2}}{2\pi\hbar^4\rho}\cdot E^{3/2}, \tag{A3}$$

where Ξ is the intraband acoustic deformation potential. The second mechanism is inelastic scattering of the electrons with neutral impurities where the conduction band electrons excite the D^0 $1S$-A_1 to T_2 transition. This is the relevant transition for the Orbach-type process. The energy relaxation rate due to collisions can be approximated by

$$\left(\frac{dE}{dt}\right)_{\text{coll}} = -\frac{\Delta}{\tau_{\text{coll}}(t)} \tag{A4}$$

for $E \geqslant \Delta$ and zero otherwise. Here, Δ is the D^0 $1S$-A_1 to T_2 transition energy. The collision rate $\tau_{\text{coll}}^{-1}(t)$ is

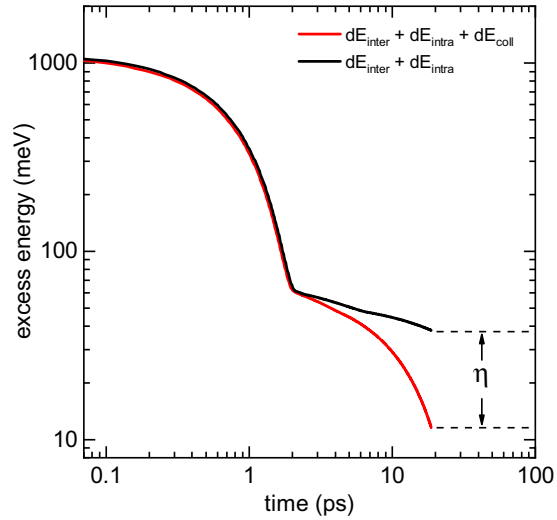

FIG. 5. Calculated dynamics of the hot Auger electrons after excitation into the conduction band. The D^0X Auger recombination defines $t = 0$. The red line depicts the calculated cooling dynamics including all relevant cooling mechanism. The black line shows the same but without inelastic D^0 scattering.

defined as

$$\frac{1}{\tau_{\text{coll}}(t)} = \sigma_{\text{coll}}\cdot v(E)\cdot n_d, \tag{A5}$$

where $\sigma_{\text{coll}} = 8 \times 10^{-12}$ cm^2 [26] and $v(E)$ is the energy-dependent velocity of the conduction band electrons calculated by the parabolic band approximation.

The red line in Fig. 5 shows the energy relaxation dynamics including intravalley scattering, intervalley scattering, and inelastic collisions with donors. After about 19 ps, the energy of the Auger electrons falls below the transition energy Δ, i.e., the energy of the conduction band electrons is not sufficient anymore for inelastic scattering with localized donor electrons involving the $1S$-A_1 to $1S$-T_2 transition. At this particular time, the energy fraction lost by the electron from its initial excess energy by inelastic collisions with donors amounts to $\eta = 26.4$ meV, i.e., each Auger electron excites according to this unpretentious calculation on average $\zeta = \eta/\Delta \approx 2.3$ $1S$-A_1 to $1S$-T_2 donor transitions.

The calculation is in surprisingly good agreement with the measured value of $\zeta = 3.2$ presented in the main text. Most importantly, the calculation shows that ζ, and thereby the Auger initiated D^0 spin relaxation rate, is rather universal and in good approximation independent of optical excitation, ionized impurity, and doping density.

[1] B. E. Kane, Nature (London) **393**, 133 (1998).

[2] A. M. Tyryshkin, S. Tojo, J. J. L. Morton, H. Riemann, N. V. Abrosimov, P. Becker, H.-J. Pohl, T. Schenkel, M. L. W. Thewalt, K. M. Itoh, and S. A. Lyon, Nature Mater. **11**, 143 (2012).

[3] P. Gumann, O. Patange, C. Ramanathan, H. Haas, O. Moussa, M. L. W. Thewalt, H. Riemann, N. V. Abrosimov, P. Becker, H.-J. Pohl, K. M. Itoh, and D. G. Cory, Phys. Rev. Lett. **113**, 267604 (2014).

[4] A. Yang, M. Steger, T. Sekiguchi, M. L. W. Thewalt, T. D. Ladd, K. M. Itoh, H. Riemann, N. V. Abrosimov, P. Becker, and H.-J. Pohl, Phys. Rev. Lett. **102**, 257401 (2009).

[5] J. J. Pla, K. Y. Tan, J. P. Dehollain, W. H. Lim, J. J. L. Morton, D. N. Jamieson, A. S. Dzurak, and A. Morello, Nature (London) **489**, 541 (2012).

[6] M. Steger, T. Sekiguchi, A. Yang, K. Saeedi, M. E. Hayden, M. L. W. Thewalt, K. M. Itoh, H. Riemann, N. V. Abrosimov, P. Becker, and H.-J. Pohl, J. Appl. Phys. **109**, 102411 (2011).

[7] M. Steger, K. Saeedi, M. L. W. Thewalt, J. J. L. Morton, H. Riemann, N. V. Abrosimov, P. Becker, and H.-J. Pohl, Science **336**, 1280 (2012).

[8] W. Schmid, Phys. Status Solidi B **84**, 529 (1977).

[9] L. Qing, J. Li, I. Appelbaum, and H. Dery, Phys. Rev. B **91**, 241405(R) (2015).

[10] The hydrostatic helium gas pressure at 4.5 K is about 1500 Pascal and can be neglected in this experiment.

[11] M. L. W. Thewalt, A. Yang, M. Steger, D. Karaiskaj, M. Cardona, H. Riemann, N. V. Abrosimov, A. V. Gusev, A. D. Bulanov, I. D. Kovalev, A. K. Kaliteevskii, O. N. Godisov, P. Becker, H. J. Pohl, E. E. Haller, J. W. A. Iii, and K. M. Itoh, J. Appl. Phys. **101**, 081724 (2007).

[12] The laser is stabilized by a temperature insulated HighFinesse wavelength meter WS-U 30. The absolute frequency is 278.033 51(1) THz.

[13] A. M. Tyryshkin, S. A. Lyon, A. V. Astashkin, and A. M. Raitsimring, Phys. Rev. B **68**, 193207 (2003).

[14] J. J. Pla, K. Y. Tan, J. P. Dehollain, W. H. Lim, J. J. L. Morton, F. A. Zwanenburg, D. N. Jamieson, A. S. Dzurak, and A. Morello, Nature (London) **496**, 334 (2013).

[15] The set of linear equations can be solved analytically but the result is bulky and therefore not shown.

[16] The kink at 0.2 W/cm^2 results from the slight energetic overlap of the doublet lines.

[17] T. G. Castner, Phys. Rev. **155**, 816 (1967).

[18] D. Karaiskaj, J. A. H. Stotz, T. Meyer, M. L. W. Thewalt, and M. Cardona, Phys. Rev. Lett. **90**, 186402 (2003).

[19] The line shape of the transition is Lorentzian for the transverse magnetic field of 50 mT. At zero magnetic field the line shape becomes a skewed Lorentzian with a low-energy tail. Such a skewed Lorentzian was observed first by A. Yang *et al.* and has been attributed to Stark broadening [23].

[20] M. Cardona, T. A. Meyer, and M. L. W. Thewalt, Phys. Rev. Lett. **92**, 196403 (2004).

[21] A. Ferrier, C. W. Thiel, B. Tumino, M. O. Ramirez, L. E. Bausá, R. L. Cone, A. Ikesue, and Ph. Goldner, Phys. Rev. B **87**, 041102(R) (2013).

[22] J. L. Cheng, J. Rioux, J. Fabian, and J. E. Sipe, Phys. Rev. B **83**, 165211 (2011).

[23] A. Yang, Ph.D. thesis, Simon Fraser University, 2010, http://summit.sfu.ca/item/11310.

[24] B. K. Ridley, *Quantum Processes in Semiconductors*, 4th ed. (Oxford University Press, Oxford, 1999).

[25] D. K. Ferry, Phys. Rev. B **14**, 1605 (1976).

[26] P. T. Greenland, S. A. Lynch, A. F. G. van der Meer, B. N. Murdin, C. R. Pidgeon, B. Redlich, N. Q. Vinh, and G. Aeppli, Nature (London) **465**, 1057 (2010).

[27] C. Jacoboni and L. Reggiani, Rev. Mod. Phys. **55**, 645 (1983).